Online Cell-by-cell SOC/SOH Estimation Method for Battery Module Employing Extended Kalman Filter Algorithm with Aging Effect Consideration

Ngoc-Thao Pham[1] · Phuong-Ha La[1] · Sung-Jin Choi[1*]

Abstract

As the number of series connections of battery cells increases, individual cells are operating in different temperature profiles, and the aging patterns of the cells become dissimilar from each other. Thenceforth, individual state-cell-characteristics should be tracked online for higher safety. Although Kalman-filter-based battery state estimation is one of the most popular methods, it is sensitive to the accuracy of the battery model parameters and difficult to be applied to every cell. This work proposes an online cell-by-cell state-of-charge (SOC)/state-of-health (SOH) estimation method to mitigate this limitation. The aging patterns of the individual cells are predicted by introducing a combination of a switch-matrix flying capacitor and electrochemical impedance spectroscopy (EIS) model parameter scanning techniques. Accordingly, the accuracy of the SOC estimation for individual cells is enhanced. The proposed method is verified by a real-time simulation platform, where the SOC and SOH levels of the cells are individually estimated within a 1.24% error.

Keywords battery cell, battery estimation, battery model, EIS, EKF calibration.

1 Introduction

The market share of the battery energy storage system (BESS) is rapidly growing [1]. In the recent electric vehicle (EV) development, a new cell-packing structure is emerging, such as a cell-to-pack technology that directly embeds the cells in the pack and eliminates modules. The battery pack is not only an enclosure but also a part of the vehicle body structure, a so-called cell-to-vehicle solution. Therefore, the number of cells connected in series is further increasing.

* Sung-Jin Choi
sjchoi@ulsan.ac.kr

1 Department of Electrical, Electronic and Computer Engineering University of Ulsan, Republic of Korea

The battery cells are screened to have similar characteristics before being grouped into a module or a pack [2]. However, this mechanism ensures the uniform performance of the cells only in the first few operation cycles, because individual cells operate in different cooling profiles, and the aging patterns of the cells are dissimilar from each other. Consequently, the estimation results for the whole battery module or pack mostly fail to represent the state of individual cells [3]. The mismatch in the battery characteristics can make the series string suffer from over-charging and over-discharging [4], because the aging patterns of the individual cells are dissimilar [5].

This type of problem is exacerbated in the second-life battery system, in which the retired battery pack from an EV is reused for BESS application. At this time, the individual cell characteristics are not as uniform as the new one [6]. Hence, the battery state of individual cells should be monitored by considering the aging characteristics of the individual cell rather than a whole battery module or pack.

Given that the state of charge level only can be estimated based on the battery voltage, current, and temperature [7], the battery state estimation techniques are actively investigated [8], [9]. For example, the Coulomb counting method estimates the SOC level of the cells by counting the amount of charge that flows into or out of the cell. This method has become the most preferred in industrial applications due to its simplicity [10], [11]. Additionally, data-driven approaches such as artificial intelligence-based techniques are also gaining popularity. The machine learning (ML) and the deep learning (DL) algorithms can accurately estimate the SOC level of the cells [12]–[14]. However, the ML-based methods require a large dataset to train the model before operation on site, and the DL-based methods demonstrate a large estimation error in the first few cycles showing a risk in safety. Meanwhile, the required computation time is considerably long to gain practical feasibility and meet the cost requirements.

On the other hand, model-based methods can estimate the SOC level with high accuracy and a low computation time [15]–[18]. For example, Kalman-filter-based battery state estimation is one of the most popular methods. However, reports indicated that these methods are sensitive to the

accuracy of the battery model parameters. The influence of battery aging on the estimation accuracy is mostly neglected, even though it is significant [19], [20]. To ensure the estimation accuracy, the battery model parameters should be online monitored to reconfigure the state space model.

In recent years, many studies apply machine learning to optimize the extended Kalman filter (EKF) algorithm. In [21], [22], the authors utilize reinforcement learning to modify the parameters of EKF. Although this approach could gain some impressive results because of self-learning ability based on real collected data, it also has the limitations of data-driven methods, such as a variety of training data, a long training time, and high computation burden.

To solve the aforementioned issues, this work proposes an effective online cell-by-cell state-of-charge (SOC)/state-of-health (SOH) estimation method for the series string. The impedance degradation of the cells is detected by utilizing an online identification method. While the SOH is estimated based on the impedance degradation, the model parameters of the individual cell are also calibrated. Besides, an EKF algorithm is used to estimate the SOC level from the updated state space model and open circuit voltage information.

After the impact of battery aging on the accuracy of the conventional Kalman filter SOC estimation is discussed in Section 2, the proposed circuit scheme and the improved estimation algorithm are explained in Section 3. The performance of the proposed method is verified by a real-time simulation platform in Section 4, and the conclusion is made in Section 5.

2 Conventional EKF-based SOC estimation and its limitation

2.1 EKF Algorithm

The EKF is suitable for a system showing a nonlinear behavior like a battery [23]. The system is linearized in real-time around the estimated state for covariance updates as the formulation from (1) to (5). Therefore, the nonlinear output is predicted and transits the state.

Prediction (time update)

- State estimation is expressed as

$$\hat{x}_{k+1|k} = A\hat{x}_{k|k} + Bu_k. \quad (1)$$

- The error covariance is calculated by

$$P_{k+1|k} = AP_{k|k}A^T + Q_k. \quad (2)$$

Correction (measurement update)

- Kalman gain is computed by

$$K_{k+1} = P_{k+1|k}C^T\left(CP_{k+1|k}C^T + R_{k+1}\right)^{-1}. \quad (3)$$

- The state variable is updated as

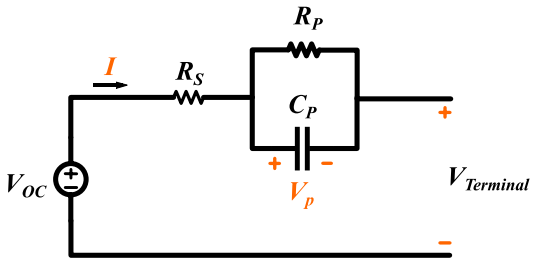

Fig. 1 Battery EIS model

$$\hat{x}_{k+1|k+1} = \hat{x}_{k+1|k} + K_{k+1}\left(z_{k+1} - C\hat{x}_{k+1|k}\right). \quad (4)$$

- The error covariance is updated by

$$P_{k+1|k+1} = (1 - K_{k+1}C)P_{k+1|k}x, \quad (5)$$

where k represents the number of iterations; x and u are the unmeasurable vector and control input vector, respectively; A is the transition matrix; B is the input matrix; C is the measurement matrix; P is the error covariance; K is the Kalman gain; z is the observed output vector; and subscripts $|k$ and $|k+1$ denote the predicted and updated values, respectively. The process noise and measurement noise covariance matrices are denoted as Q and R, respectively.

The battery cell is modeled by a Thevénin equivalent circuit, as shown in Fig. 1, which is called the EIS model in this work. Although the second order model can achieve higher accuracy, its computation becomes complex. Accordingly, the first order model is chosen for the state estimation for individual cells. The model consists of an open circuit voltage (V_{OC}) and an R-RC (R_s, R_p, C_p) equivalent impedance circuit. The battery SOC is computed by the ratio of the remaining capacity to the total capacity as

$$SOC(k+1) = SOC(k) - \frac{\eta \Delta t\, i(k)}{C_n}. \quad (6)$$

Meanwhile, the terminal voltage of the cell is calculated by

$$V_t(k) = V_{OC}(k) - V_P(k) - i(k)R_S, \quad (7)$$

where $V_{OC}(k)$ is the open-circuit voltage at the kth sampling time and is a function of SOC, $V_p(k)$ is the polarization voltage at the kth sampling time applied to the parallel RC network, η is the efficiency of charge/discharge process, $i(k)$ denotes the measured current of the cell, C_n is the nominal full capacity of the cell, and Δt is the sample time. For a convention, the polarity of the charging and discharging current are regarded as positive and negative, respectively. Thus, the polarization voltage at the $(k+1)$th sample is calculated by

$$V_P(k+1) = e^{\frac{-\Delta t}{R_P C_P}}V_P(k) - R_p\left(1 - e^{\frac{-\Delta t}{R_P C_P}}\right)i(k). \quad (8)$$

In the battery system, (6) and (8) are the state equations, while (7) is the output equation. By linearizing this system, the state space equation of SOC and V_p are built in as follows:

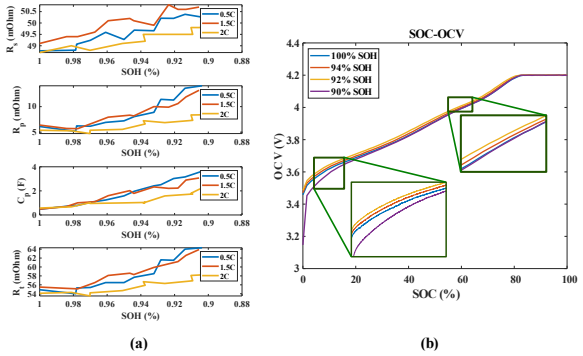

Fig. 2 Changes in the battery characteristics during aging: **a** battery impedance; **b** SOC–OCV

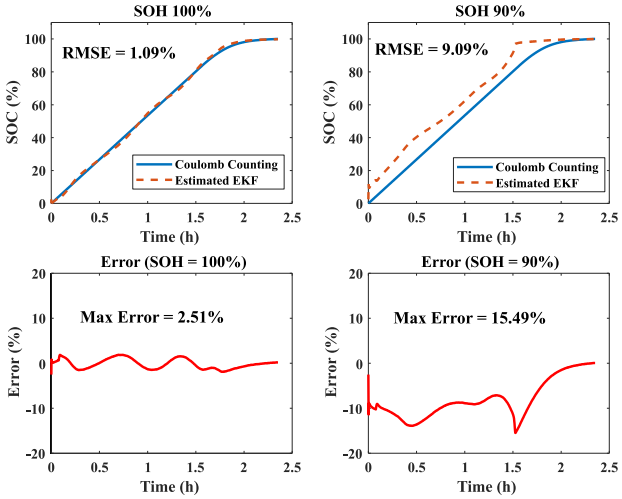

Fig. 3 SOC estimation without model calibration at 100% and 90% SOH

$$\begin{bmatrix} SOC \\ V_p \end{bmatrix}_{k+1} = A_k \begin{bmatrix} SOC \\ V_p \end{bmatrix}_k + B_k i_k. \quad (9)$$

Meanwhile, the output vector V_t is expressed as

$$V_t(k) = C_k \begin{bmatrix} SOC \\ V_p \end{bmatrix}_k + D_k i_k, \quad (10)$$

where Jacobian matrices A_k, B_k, C_k, and D_k are expressed as:

$$A_k = \begin{bmatrix} 1 & 0 \\ 0 & e^{\frac{-\Delta t}{R_p C_p}} \end{bmatrix}, \quad (11)$$

$$B_k = \begin{bmatrix} -\frac{\Delta t\, \eta(k)}{C_n} \\ R_p\left(1 - e^{\frac{-\Delta t}{R_p C_p}}\right) \end{bmatrix}, \quad (12)$$

$$C_k = \begin{bmatrix} \frac{\partial V_{OC}}{\partial SOC} & -1 \end{bmatrix}, \quad (13)$$

$$D_k = -R_S. \quad (14)$$

The state space models of the EKF are strongly dependent on the EIS model parameters (R_s, R_p, and C_p) in Fig. 1, the actual capacity (C_n), and the OCV–SOC relationship of the cells at the current conditions, most of which are affected by aging.

2.2 Necessity of cell-by-cell aging effect consideration

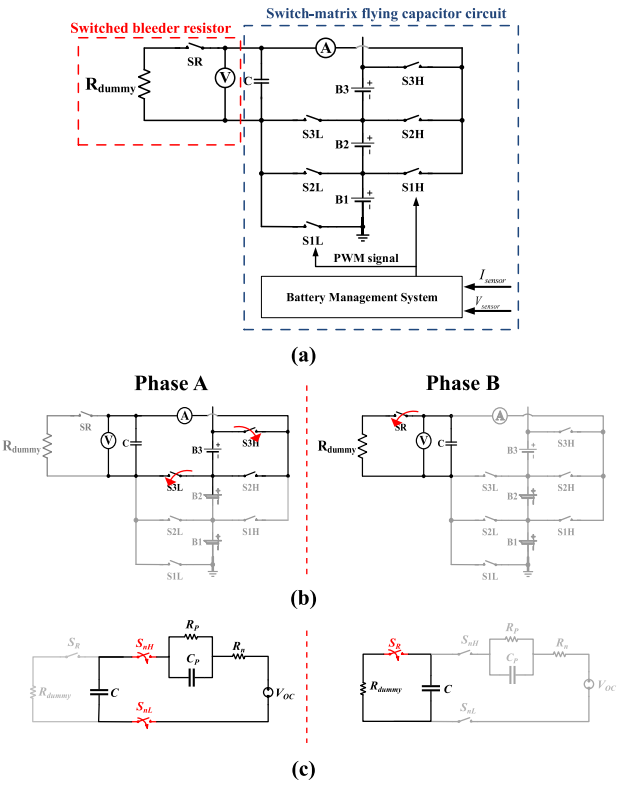

Fig. 4 Proposed cell-by-cell parameter extraction: **a** switch matrix circuit; **b** operation of cell #3; **c** equivalent circuit of the identification process

To further investigate the influence of aging on the EKF estimation accuracy, multiple tests have been conducted to observe the battery characteristic at the various SOH levels. The device under test is the 18650 Li-ion Samsung SDI (3.6V/2.9Ah) cells. The cells are fully charged at 0.5C-rate current and are discharged by various C-rates (0.5C, 1.5C, and 2C) at 25 °C ambient temperature. The battery cells are gradually aged by repeating the tests. After every 50 cycles, the battery impedance and OCV–SOC relationship of the cells are observed to form the historical dataset of the cells at the various SOH levels.

The changes in the battery impedance and OCV–SOC mapping curve are illustrated in Fig. 2. According to the results, the battery impedance drifted by 15% from the initial condition after 550 cycles. Meanwhile, the OCV–SOC curve deviates from the initial curve. Both factors significantly reduce the accuracy of the EKF estimation.

The same EKF estimator has been applied for the charging process of a cell at 100% and 90% SOH levels. The estimation results are compared with the reference value from the cycler in Fig. 3. The maximum error increased from 2.51% (at 100% SOH) to 15.49% (at 90% SOH). Evidently, the aging of the cell increases the error of the EKF estimator.

On the other hand, the aging pattern of the cells is different from each other even under the same driving

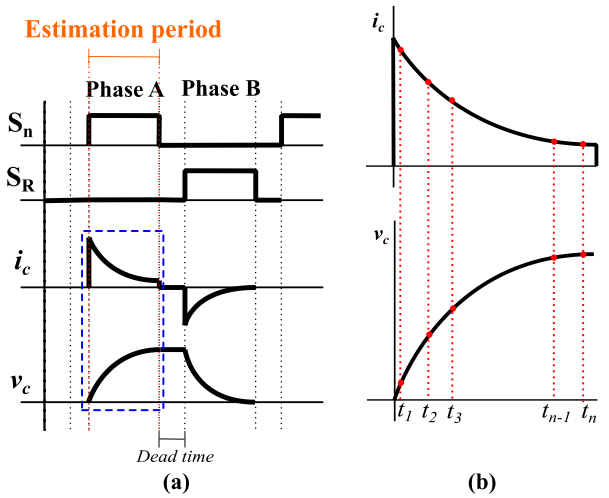

Fig. 5 Theoretical waveforms: **a** current and voltage of the measuring capacitor; **b** multiple measurement points

condition [24]. Consequently, the assessment of the whole pack by a single EKF estimation becomes inappropriate. Therefore, online cell-by-cell state estimation is essential.

3 Proposed method

In this section, the proposed method is developed for a switch-matrix flying capacitor circuit that is connected in turns to the individual cells. Most of the equivalent model parameters of the cells can be estimated based on the charge transfer theory of the switched capacitor circuit. Thenceforth, the impedance degradation is detected to interpolate the SOH level. The corresponding OCV–SOC relationship and the state space model of the EKF are reconfigured based on the estimated SOH level. In virtue of the switch-matrix, the estimation process can be implemented for the individual cells one by one.

3.1 Online cell-by-cell parameter extraction

The online identification method is implemented on the switch-matrix flying capacitor circuit, which is illustrated in Fig. 4a. The hardware consists of a switch-matrix, a flying capacitor, and a switched bleeder resistor. The charge transfer process is divided into two phases, as shown in Fig. 4b–c. The parameters of the EIS model are extracted in phase A (t_0–t_1), where one cell is connected to the capacitor, C. In phase B (t_2–t_3), the capacitor is fully discharged by a switched bleeder resistor circuit before the next measurement starts.

According to the analysis in [25], the current flow through the loop is expressed by

$$i_C(t) = \frac{\Delta V}{R_n+R_p}\left(1+\frac{R_p}{R_n}e^{\frac{-(R_n+R_p)t}{R_nR_pC_p}}\right), \quad (15)$$

$$\Delta V = V_{OC} - v_C(t), \quad (16)$$

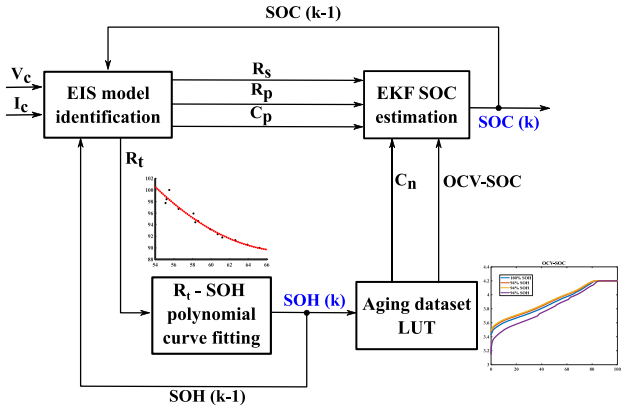

Fig. 6 Proposed SOC/SOH estimation algorithm

where the V_{OC} is the open-circuit voltage of the battery, which is measured in the initial process; $v_C(t)$ and $i_C(t)$ are the measured voltage and current of the capacitor at time t, respectively; R_n is the sum of the model serial resistance and the circuit resistance (including the ESR of the capacitor, on-resistance of switches, and shunt resistance). The theoretical waveforms of the capacitor current and voltage are shown in Fig. 5a.

R_n, R_p, and C_p are identified by assessing the capacitor current and voltage at multiple points. After reformulating (15) into

$$\frac{i_C(t)}{\Delta V} = \frac{1}{R_n+R_p} + \frac{R_p}{R_n(R_n+R_p)}e^{\frac{-(R_n+R_p)t}{R_nR_pC_p}} \quad (17)$$

and applying the exponential curve fitting to (17), the current (i_C) and voltage (v_C) of the equalization capacitor at the various points (Fig. 5b) are utilized to calculate the parameters of the EIS model. From the extracted EIS model parameters (R_s, R_p, C_p), the total resistance of the cell (R_t) is calculated by

$$R_t = R_s + R_p. \quad (18)$$

3.2 Parameter reconfiguration for EKF considering the aging effects

The parameter reconfiguration process of one cell is demonstrated in Fig. 6. In the EIS model identification block, the model parameters of the cell are identified, as mentioned in Section 3.1. Accordingly, the EIS model is utilized to update the state space model for SOC estimation. Next, the correlation between SOH level and R_t is illustrated in Fig. 7 based on the historical dataset in Section 2.2. The SOH level is a function of R_t, which can be derived by applying the polynomial curve fitting technique. Therefore, the SOH level is estimated directly from the measured R_t. In this work, the relation is obtained as:

$$SOH = 0.05347 \times R_t^2 - 7.138 \times R_t + 339.8. \quad (19)$$

This relation is used for constructing the aging dataset look-up table, where the corresponding actual capacity (C_n) and SOC–OCV relationship are calculated based on the

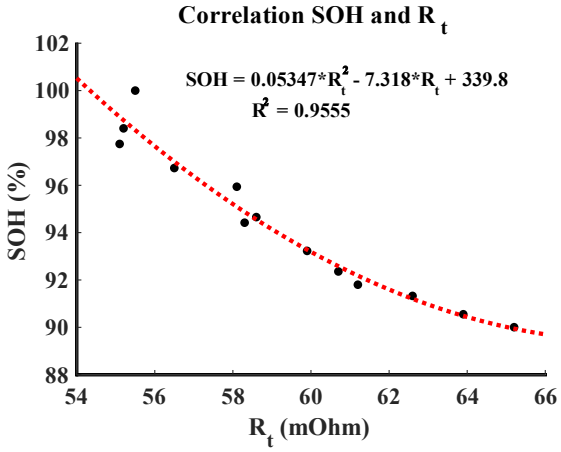

Fig. 7 Correlation SOH and R_t

SOH level. Finally, the updated C_n and SOC–OCV relationship are simultaneously utilized for the EKF estimator to estimate the SOC level.

After the model parameters for one cell are obtained, the switch-matrix is controlled to dock other cells to the flying capacitor for another parameter extraction step. Because the SOH slowly decreases by nature, this process can be conducted in the idle mode of the cells; right before every charging process or during any usual battery maintenance routine. The extra computation time or energy loss is trivial because the whole reconfiguration process is considerably fast and seldom occurs.

4 Real-time test results

First, the reference set should be constructed. The reference SOC and SOH levels of the cells are calculated based on the actual capacity of the cells, which are provided by the Coulomb counting method with a very high accuracy sensing equipment Maccor 4300K. The battery is repeatedly charged and discharged by a battery cycler (a Maccor 4300K) at 25 °C ambient temperature. The cells are charged in CC at 0.5C-rate current and in CV at 4.2 V with 0.02C-rate cut-off current. The cells are discharged by CC at a 1.5C-rate with a 2.5 V cut-off voltage. The cell model parameters are extracted every 50 cycles by using the sinusoidal injection method with a genetic estimation algorithm to create a reference set of data for the EIS model. This method is supplied by the commercial offline EIS measurement equipment (ZIVE SP10).

The accuracy of the model parameters is evaluated with an FPGA-based real-time hardware-in-the-loop test platform (Typhoon HIL 602+). Based on the reference parameters from the EIS test rests, the circuit model is constructed into a real-time platform to isolate the effects of unintended disturbances, such as temperature changes during the operation and manufacturing tolerances in battery characteristics. Then, the proposed method is

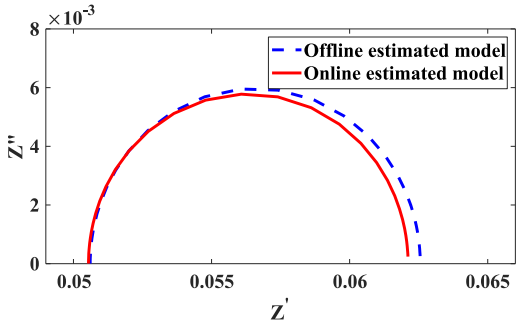

Fig. 8 Cole–Cole plot of the impedance of cell #3

implemented in the real-time platform, and the algorithm is executed for a 3S1P battery string consisting of three cells in series. The estimated parameters are summarized in Table 1.

Table 1 Estimated parameters of the EIS-model

	R_s (mΩ)	R_p (mΩ)	R_t(mΩ)	C_p (F)
Sample #1	49.4	5.70	55.1	1.0279
(%Error)	(0.064)	(0.18)	(0.0004)	(1.87)
Sample #2	50.73	10.03	60.77	2.13
(%Error)	(0.04)	(1.34)	(0.04)	(3.54)
Sample #3	50.55	11.57	62.12	2.87
(%Error)	(0.12)	(3.18)	(0.02)	(1.02)

According to the comparison of the extracted parameters with the reference value from the commercial EIS equipment, the maximum errors in the estimation are 0.12% for R_s, 3.18% for R_p, 0.04% for R_t, and 3.54% for C_p, respectively. The impedance of the equivalent circuit with the extracted parameter is plotted under a frequency-sweep sequence in Fig. 8. The Cole–Cole plot of sample #3 at 91.3% the SOH condition shows that the online extraction data obtained by the proposed method matches well with the reference curve generated by the commercial offline equipment. Thus, the EKF parameters, such as R_s, R_p, and C_p, can be successively reconfigured.

Meanwhile, the actual SOH level is predicted by the proposed algorithm based on the estimated impedance of the cells and the dataset. The predicted values are summarized in Table 2, where the proposed method can predict the SOH level within 1.2% error, showing that the proposed method efficiently performs in predicting the SOH condition of the cells. In this case, the remaining EKF parameters, such as OCV–SOC relation and C_n, can be obtained.

Table 2 SOH estimation result by the proposed method

Sample	$R_{t\_reference}$ (mΩ)	$R_{t\_estimated}$ (mΩ)	SOH_{ref} (%)	$SOH_{estimated}$ (%)	SOH_{error} (%)
Sample #1	55.12144	55.1	97.74741	98.9137	1.1931
Sample #2	60.65297	60.766	92.35813	92.5527	0.2107
Sample #3	62.55597	62.115	91.32608	91.5443	0.2389

Thenceforth, EKF parameters reflect the aging effects, and the SOC estimation accuracy is greatly improved. To

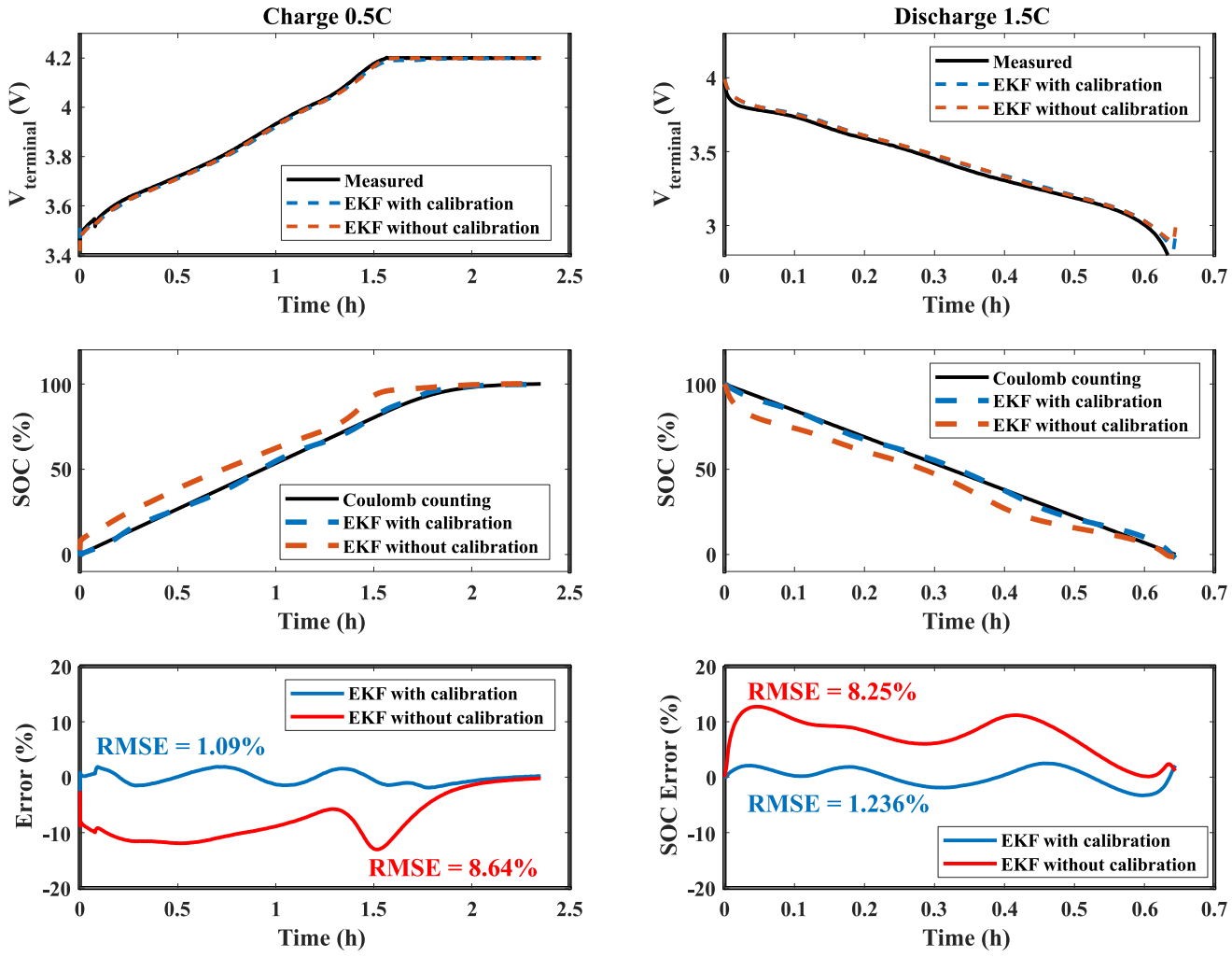

Fig. 9 SOC estimation result at 91.3% SOH

closely investigate the performance, the EKF estimation with or without the state space parameters reconfiguration is tested for a 0.5C-rate charging and 1.5C-rate discharging process of sample #3 at the 550th cycle (91.3% SOH). The SOC estimation error is assessed by root-mean-square-error (RMSE), which is calculated by

$$RMSE = \sqrt{\frac{(SOC_{ref} - SOC_{estimated})^2}{N}}, \qquad (20)$$

where SOC_{ref} and $SOC_{estimated}$ are the reference SOC and the estimated SOC, respectively; and N is the number of data.

The terminal voltage and SOC profile of the battery cell are illustrated in Fig. 9. The EKF estimation without the aging consideration has a high RMSE in SOC estimation (8.64% during the charging and 8.26% during the discharging process). By contrast, the estimation error is reduced below 1.24% RMSE because the model parameter is extracted online and cell-by-cell. Therefore, the state space parameter reconfiguration process is effective in improving the accuracy of the SOC estimation for individual cells.

5 Conclusion

By considering the battery aging, the online cell-by-cell parameter extraction technique for the individual cell is proposed along with a switch matrix flying capacitor structure. The SOC and SOH levels are obtained by tracking the actual model parameters of the individual cells. The verification result proves that the EKF estimation combined with the proposed state space parameter reconfiguration process can effectively improve the estimation accuracy. Furthermore, the proposed circuit structure is simple enough to be integrated into conventional active cell balancing circuits.

Acknowledgments

This work was partly supported by the Technology Development Program (S3207312) funded by the Ministry of SMEs and Startups (MSS, Korea) and the National Research Foundation of Korea (NRF-2020R1A2C2009303) grant funded by the Korea government (MSIT).

References

1. Castillo, G. A. L., Alava, L. A. C., Arauz, W. M. S., & Rodríguez, J. A. P.:Proposal of photovoltaic system for house. International Journal of Physical Sciences and Engineering, 4(2), 26–35 (2020).
2. Kim, J., & Cho, B. H.: Screening process–based modeling of the multi–cell battery string in series and parallel connections for high accuracy state–of–charge estimation. Energy, 57, 581–599 (2013).
3. Dong, H., Huang, W., & Zhao, Y.: Low complexity state–of–charge estimation for lithium–ion battery pack considering cell inconsistency. Journal of Power Sources, 515, 230599 (2021).
4. Guo, R., Lu, L., Ouyang, M., & Feng, X.: Mechanism of the entire overdischarge process and overdischarge–induced internal short circuit in lithium–ion batteries. Scientific reports, 6(1), 1–9 (2016).
5. Zhang, C., Jiang, Y., Jiang, J., Cheng, G., Diao, W., & Zhang, W.: Study on battery pack consistency evolutions and equilibrium diagnosis for serial–connected lithium–ion batteries. Applied Energy, 207, 510–519 (2017).
6. Martinez–Laserna, E., Gandiaga, I., Sarasketa–Zabala, E., Badeda, J., Stroe, D. I., Swierczynski, M., & Goikoetxea, A.: Battery second life: Hype, hope or reality? A critical review of the state of the art. Renewable and Sustainable Energy Reviews, 93, 701–718 (2018).
7. Chen, Y., Kang, Y., Zhao, Y., Wang, L., Liu, J., Li, Y., ... & Li, B.: A review of lithium–ion battery safety concerns: The issues, strategies, and testing standards. Journal of Energy Chemistry, 59, 83–99 (2021).
8. Park, S., Ahn, J., Kang, T., Park, S., Kim, Y., Cho, I., & Kim, J.: Review of state–of–the–art battery state estimation technologies for battery management systems of stationary energy storage systems. Journal of Power Electronics, 20(6), 1526–1540 (2020).
9. Xiong, R., Cao, J., Yu, Q., He, H., & Sun, F.: Critical review on the battery state of charge estimation methods for electric vehicles. IEEE Access, 6, 1832–1843 (2017).
10. Ng, K. S., Moo, C. S., Chen, Y. P., & Hsieh, Y. C.: Enhanced coulomb counting method for estimating state–of–charge and state–of–health of lithium–ion batteries. Applied Energy, 86(9), 1506–1511 (2009).
11. Zhao, L., Lin, M., & Chen, Y.: Least-squares based coulomb counting method and its application for state-of-charge (SOC) estimation in electric vehicles. International Journal of Energy Research, 40(10), 1389–1399 (2016).
12. Salkind, A. J., Fennie, C., Singh, P., Atwater, T., & Reisner, D. E.: Determination of state–of–charge and state–of–health of batteries by fuzzy logic methodology. Journal of Power sources, 80(1–2), 293–300 (1999).
13. Shen, W. X., Chan, C. C., Lo, E. W. C., & Chau, K. T.: A new battery available capacity indicator for electric vehicles using neural network. Energy Conversion and Management, 43(6), 817–826 (2002).
14. Hansen, T., & Wang, C. J.: Support vector based battery state of charge estimator. Journal of Power Sources, 141(2), 351–358 (2005).
15. Plett, G. L.: Extended Kalman filtering for battery management systems of LiPB–based HEV battery packs: Part 3. State and parameter estimation. Journal of Power sources, 134(2), 277-292 (2004).
16. Pulavarthi, C., Kalpana, R., & Parthiban, P.: State of Charge estimation in Lithium-Ion Battery using model based method in conjunction with Extended and Unscented Kalman Filter. In 2020 International Conference on Power Electronics and Renewable Energy Applications (PEREA) (pp. 1-6). IEEE (2020, November).
17. Jokić, I., Zečević, Ž., & Krstajić, B.: State–of–charge estimation of lithium–ion batteries using extended Kalman filter and unscented Kalman filter. In 2018 23rd International Scientific–Professional Conference on Information Technology (IT) (pp. 1–4). IEEE (2018, February).
18. Khanum, F., Louback, E., Duperly, F., Jenkins, C., Kollmeyer, P. J., & Emadi, A.: A Kalman filter based battery state of charge estimation MATLAB function. In 2021 IEEE Transportation Electrification Conference & Expo (ITEC) (pp. 484–489). IEEE (2021, June).
19. Pop, V., Bergveld, H. J., Regtien, P. P., het Veld, J. O., Danilov, D., & Notten, P. H. L.: Battery aging and its influence on the electromotive force. Journal of The Electrochemical Society, **154**(8), A744 (2007).
20. Xiong, R., Pan, Y., Shen, W., Li, H., & Sun, F.: Lithium–ion battery aging mechanisms and diagnosis method for automotive applications: Recent advances and perspectives. Renewable and Sustainable Energy Reviews, 131, 110048 (2020).
21. Kim, M., Kim, K., Kim, J., Yu, J., & Han, S.: State of charge estimation for lithium Ion battery based on reinforcement learning. IFAC–PapersOnLine, **51**(28), 404–408 (2018).
22. You, G., Wang, X., Fang, C., Zhang, S., & Hou, X.: State of charge estimation of lithium–ion battery based on double deep Q network and extended Kalman filter. In IOP Conference Series: Earth and Environmental Science (Vol. 615, No. 1, p. 012080).

IOP Publishing (2020, December).
23. Chui, C. K., & Chen, G.: Extended Kalman filter and system identification. In Kalman Filtering (pp. 115–137). Springer, Cham (2017).
24. Gong, X., Xiong, R., & Mi, C. C.: Study of the characteristics of battery packs in electric vehicles with parallel–connected lithium–ion battery cells. IEEE Transactions on Industry Applications, **51**(2), 1872–1879 (2014).
25. La, P. H., & Choi, S. J.: Direct Cell–to–Cell Equalizer for Series Battery String Using Switch–Matrix Single–Capacitor Equalizer and Optimal Pairing Algorithm. IEEE Transactions on Power Electronics, **37**(7), 8625–8639 (2022).

Ngoc–Thao Pham received her B.S Degree in Electrical Engineering from Ho Chi Minh City University of Technology (HCMUT), Vietnam National University, Ho Chi Minh City, Vietnam in 2019. After graduating, she worked as a Software engineer with Greystone Data System Vietnam. She is currently enrolled in a Master's degree program. Her current research interests include Battery Management Systems: EIS model identification for battery and battery state estimation.

Phuong–Ha La received his B.S. degree in Automation and Control Systems from the Ho Chi Minh City University of Technology, Vietnam National University, Ho Chi Minh City, Vietnam, in 2014. He worked as an R&D and Project Management Specialist with Dien Quang Lamp JSC, Ho Chi Minh City, Vietnam from 2013 to 2017. He is currently pursuing his Ph.D. degree at the Energy Conversion Circuit Laboratory, University of Ulsan, Ulsan, South Korea. His current research interests include battery management systems, battery chargers, and cell balancing.

Sung–Jin Choi received his B.S., M.S., and Ph.D. degrees in Electrical Engineering from Seoul National University, Seoul, South Korea, in 1996, 1998, and 2006, respectively. He worked as a Research Engineer with Palabs Company Ltd., Seoul, South Korea from 2006 to 2008. From 2008 to 2011, he was the Principal Research Engineer of Samsung Electronics Company Ltd., Suwon, South Korea, where he was responsible for developing LED drive circuits and wireless battery charging systems. In 2011, he joined the University of Ulsan, Ulsan, South Korea, where he is currently as a Professor in the Department of Electrical, Electronic and Computer Engineering. He was a Visiting Scholar at San Diego State University, San Diego, CA, USA from 2017 to 2018 and at the University of Colorado Denver, Denver, CO, USA in 2022. Dr. Choi is the Editor of the Journal of Power Electronics. His current research interests include modeling and control of high–frequency power converters in solar power generation, battery management, and wireless power transfer.